



Charge-Transfer Character Drives Möbius Antiaromaticity in the Excited Triplet State of Twisted [28]Hexaphyrin

Ema, Fumitoshi ; Tanabe, Mana ; Saito, Shohei ; Yoneda, Tomoki ; Sugisaki, Kenji ; Tachikawa, Takashi ; Akimoto, Seiji ; Yamauchi, Seig...

(Citation)

Journal of Physical Chemistry Letters, 2018(9):2685-2690

(Issue Date)

2018-05-09

(Resource Type)

journal article

(Version)

Accepted Manuscript

(Rights)

© 2018 American Chemical Society

(URL)

<https://hdl.handle.net/20.500.14094/90004825>



Charge-Transfer Character Drives Möbius Antiaromaticity in the Excited Triplet State of Twisted [28]Hexaphyrin

Fumitoshi Ema,[†] Mana Tanabe,^{§,‡} Shohei Saito,[‡] Tomoki Yoneda,^{‡,‡} Kenji Sugisaki,[¶] Takashi Tachikawa,^{†,‡} Seiji Akimoto,[†] Seigo Yamauchi,^{§,#} Kazunobu Sato,^{,¶} Atsuhiko Osuka,^{*,‡} Takeji Takui,^{*,¶} and Yasuhiro Kobori^{*,†,‡}.*

[†]Department of Chemistry, Graduate School of Science, Kobe University, 1-1 Rokkodai-cho, Nada-ku, Kobe 657-8501, Japan

[§]Institute of Multidisciplinary Research for Advanced Materials, Tohoku University, Katahira 2-1-1, Aoba-ku, Sendai 980-8577, Japan

[‡]Department of Chemistry, Graduate School of Science, Kyoto University, Sakyo-ku, Kyoto 606-8502, Japan

[¶]Department of Chemistry and Molecular Materials Science, Graduate School of Science, Osaka City University, 3-3-138 Sugimoto, Sumiyoshi-ku, Osaka 558-8585, Japan

[‡]Molecular Photoscience Research Center, Kobe University, 1-1 Rokkodai-cho, Nada-ku, Kobe 657-8501, Japan

AUTHOR INFORMATION

Corresponding Author

*Email: sato@sci.osaka-cu.ac.jp

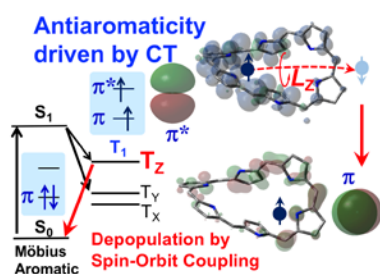
*Email: osuka@kuchem.kyoto-u.ac.jp

*Email: takui@sci.osaka-cu.ac.jp

*Email: ykobori@kitty.kobe-u.ac.jp

ABSTRACT: Möbius aromatic molecules have attracted great attention as new functional materials because of their π -orbital cyclic conjugations lying along the twisted Möbius topology. To elucidate the electronic character of the lowest excited triplet (T_1) state of a Möbius aromatic [28]hexaphyrin, we employed a time-resolved electron paramagnetic resonance (TREPR) method with applying magnetophotoselection measurements at 77 K. Analyses of the EPR parameters have revealed that the T_1 state possesses an intramolecular charge-transfer (CT) character together with a local excitation character residing at one side in the Möbius strip ring. We have also demonstrated that the CT character between orthogonal unpaired orbitals triggers a quick triplet deactivation by the spin-orbit coupling. This deactivation can be an important barometer to represent the “antiaromaticity” because of a connection between the orthogonal CT character and instability by a weakened spin-spin exchange coupling in the T_1 state.

TOC GRAPHICS



Aromaticity is one of the most common concepts that plays an important role in chemistry.¹⁻⁷ Chemical properties and reactivities of π -conjugated macrocyclic molecules depend on their aromatic or antiaromatic character.^{8,9} As a complement of the Hückel rule,¹⁰ Heilbronner predicted that $[4n]$ and $[4n+2]$ π -electronic systems with singly twisted topology show aromaticity and antiaromaticity, respectively.¹¹ The aromatic molecules show diatropic ring currents, negative nucleus-independent chemical shift (NICS) values at the ring center, and large harmonic oscillator model of aromaticity (HOMA) values.¹² In recent years, Möbius aromatic macrocyclic molecules have been extensively synthesized.¹³⁻¹⁶ Their aromatic or antiaromatic characters have been confirmed experimentally in the singlet S_0 states,¹⁷⁻²¹ but their excited electronic properties, particularly in T_1 states have been scarcely studied so far. Expanded porphyrins²²⁻²⁶ have attracted great attention. Importantly, some expanded porphyrins have been shown to take on twisted conformations exhibiting the Möbius aromaticity or antiaromaticity.^{15-17,21,23,26} Meso-aryl-substituted hexaphyrin(1.1.1.1.1.1)s can be a $[26]$ or $[28]$ π -electronic state.^{18,27,28} Planar $[26]$ hexaphyrin and $[28]$ hexaphyrin display aromatic and antiaromatic characters, respectively, in the S_0 states.^{17,18,21} These aromatic and antiaromatic natures are reversed in the T_1 state.^{20,29,30} The excited state aromaticity/antiaromaticity of twisted hexaphyrins has received much attention in relation with the Baird's rule.³¹⁻³⁴ Detailed electronic structures associated with the aromaticity/antiaromaticity, however, have not been investigated in the twisted Möbius aromatic molecules in the T_1 state. In this study, we examined the T_1 states of the meso-hexakis(pentafluorophenyl) $[26]$ hexaphyrin(1.1.1.1.1.1) **[26]Hex** and of the meso-hexakis(pentafluorophenyl) $[28]$ hexaphyrin (1.1.1.1.1.1) **[28]Hex** (Figure 1) using an X-band time-resolved electron paramagnetic resonance (TREPR) method in combination with

magnetophotoselection (MPS) measurements. We show that the unpaired electronic orbitals in the T_1 state are not uniformly delocalized over the macrocycle of the twisted Möbius [28]hexaphyrin at cryogenic temperature.

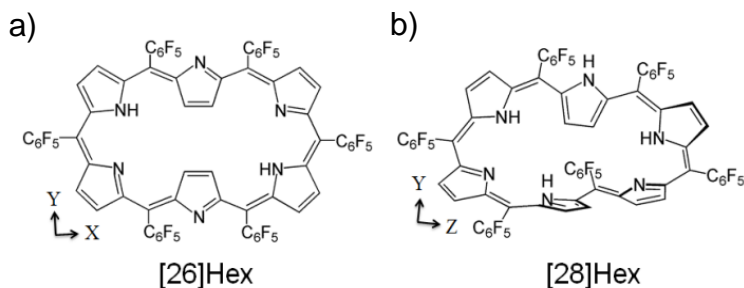


Figure 1. Molecular Structures of [26]Hex and [28]Hex.

Figure 2 shows the delay-time-dependent TREPR spectra of [28]Hex obtained by irradiating the depolarized light, the light (L) parallel to B_0 ($L // B_0$), and the light perpendicular to B_0 ($L \perp B_0$). The symmetrical broad EPR spectrum lines were found to be highly dependent upon both the L direction and the delay time. The magnetophotoselection effects denote that the broad TREPR spectra originate from peak splittings by the anisotropic spin-spin dipolar coupling in the T_1 state as the zero-field splitting (ZFS) interaction whose tensor orientation is defined with respect to the optical transition dipole moment in the molecule.^{35,36} The identifications of the ZFS tensor can thus be performed by the analysis of the TREPR spectra, enabling us to characterize the electronic structures of the T_1 states. The ZFS parameters of D and E are defined in the spin-spin dipolar interaction³⁷ as, $D = 3(g\beta)^2 \langle (r_{12}^2 - z_{12}^2)/r_{12}^5 \rangle / 4$ and $E = 3(g\beta)^2 \langle (y_{12}^2 - x_{12}^2)/r_{12}^5 \rangle / 4$, where x_{12} , y_{12} and z_{12} are axis components in the separation vector r_{12} between the two spins (1 and 2) in the principal axes system (X, Y, Z) of the triplet state. We performed model calculations of the TREPR spectra based on the line-shape theory for the triplet state, as reported by Levanon.³⁸ Details of the line-shape analyses are described in Supporting

Information (SI). The spin polarization of the microwave absorption (A) and the emission (E) is caused by the anisotropy in the initial sublevel populations P_X , P_Y , and P_Z in the zero-field spin wave functions of T_X , T_Y , and T_Z by the intersystem crossing (ISC).³⁹ The TREPR spectra of **[28]Hex** observed in toluene at 0.5 μs (Figure 2a-c) exhibit the E/A/E/A/E/A polarization pattern. The ZFS parameters of **[28]Hex** were obtained to be $|D| = 532 (\pm 3)$ MHz and $|E| = 18.2 (\pm 2)$ MHz. The ZFS parameters of **[26]Hex** (See Figure S1 for details.) and of a butadiyne-substituted free base diarylporphyrin (H_2P)³⁹ are also listed in Table 1.

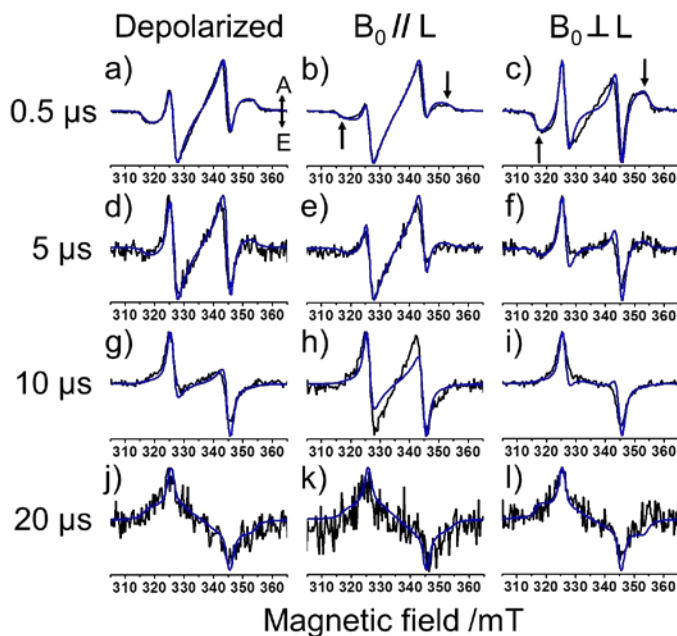


Figure 2. Experimental (black) and simulated (blue) TREPR spectra of **[28]Hex** observed at several delay times after the 650 nm laser irradiations at 77 K in toluene. Depolarized light was employed in the left. $B_0 // L$, and $B_0 \perp L$ denote that the polarization directions of the laser light (L) were parallel and perpendicular to the external magnetic field (B_0), respectively.

The $|E|$ value in **[28]Hex** is significantly smaller than those of **[26]Hex** and H_2P , denoting a negligibly small spin-density distribution difference between the X and Y directions in the

[28]Hex molecule. Since **[26]Hex** is the planar molecule²⁸ as well as H₂P, the D value of **[26]Hex** is expected to be positive ($D > 0$) because of $r_{12}^2 > 3z_{12}^2$.^{40,42,43} In this case, the principal Z-axis is directing to the out-of-plane while the X- and Y-axes are located at in-planes of

Table 1. ZFS parameters (D and E) and anisotropies ($P_x : P_y : P_z$) of the populations at the zero-field sublevels in **[26]Hex**, **[28]Hex**, H₂P, and carotenoid.

	D / MHz	E / MHz	$ E/D $	$P_x : P_y : P_z$
[26]Hex ^a	813(± 3)	-205(± 3)	0.25	0.05:0.95:0.00
[28]Hex ^b	-532(± 3)	-18.2(± 2)	0.034	0.00:0.60:0.40
H ₂ P ^c	1024(± 3)	-144(± 2)	0.14	0.47:0.53:0.00
Carotenoid ^d	-1160(± 2)	-114(± 2)	0.098	0.40:0.20:0.40

^a In MTHF. ^b In toluene. ^c Taken from reference 40. ^d Taken from reference 41. The negative D is conclusive for $P_x : P_y : P_z = 0.4:0.2:0.4$ to account for the E/E/A/E/A/A polarization generated by the triplet-triplet energy transfer.

[26]Hex in Figure 1a.^{42,43} Thus, the large $|E|$ value in **[26]Hex** is rationalized by the delocalized electronic distribution for the planar rectangular π -skeleton. This well supports the larger $|E/D|$ value in **[26]Hex** than $|E/D|$ in H₂P in Table 1, since H₂P is rather square-shaped. Under the present cryogenic conditions, the twisted conformation is predominant in **[28]Hex** as confirmed by the ground state absorption spectrum in Figure S2 and S3²⁷. The quite small $|E|$ value in comparison to $|D|$ ($|E/D| = 0.0342$) in **[28]Hex** in Table 1 thus suggests that the unpaired

electrons are not delocalized in the disordered molecular framework in Figure 1b. The small $|E/D|$ also excludes conformation changes of the twisted $^3[28]\text{Hex}^*$ to yield the planar $^3[28]\text{Hex}^*$ at 77K.²⁷ One possible explanation of this small $|E|$ is that the unpaired electrons are separated from each other as a charge-transfer (CT) state, resulting in $\langle(y_{12}^2 - x_{12}^2)/r_{12}^5\rangle \approx 0$ in E due to the twisted framework. If the two spins are separated, $D < 0$ is expected in $[28]\text{Hex}$. The other possible explanation would be that the two unpaired spins are both locally distributed at one side of the twisted ring of $[28]\text{Hex}$. If these electrons reside along a long axis (Z) like the spin density distribution in the excited triplet state of carotenoid, the negative D is also expected.^{41,44,45}

The molecular orbital (MO) calculations were carried out for the planar $[26]\text{Hex}$ and the twisted Möbius $[28]\text{hex}$ in the T_1 states, as detailed in section 1-4 of SI. In the MO calculations, the pentafluorophenyl groups in Figure 1 were replaced by hydrogen atoms, as model molecules. The gross spin density distributions calculated by the CIS method (CIS/cc-pVDZ) denoted a delocalized character in planar $[26]\text{Hex}$ (Figure S4a). This well explains the positive D value together with the larger $|E|$ value of the rectangular molecule than that of $^3\text{H}_2\text{P}$ in Table 1. On the other hand, the twisted Möbius $[28]\text{Hex}$ exhibited a localized spin density distribution (Figure S4b), indicating that the two unpaired spins are located at one side of the strip ring, as the local excitation (LE) state. From computed configuration interaction (CI) coefficients, as detailed in Figure S5, the contributions of the CT and LE characters were estimated to be ca. CT:LE = 1:5 in the twisted Möbius $[28]\text{Hex}$. These LE and CT characters are both consistent with the anticipated negative D value.

To determine the orientation of the principal \mathbf{D} -tensor axes with respect to the transition dipole moment (\mathbf{M}) in $[28]\text{Hex}$, the MPS analyses were examined in Figure 2 at 0.5 μs .⁴⁶⁻⁴⁸ In

the present MPS measurements, the 650 nm light was selected to photoexcite **[28]Hex** based on the UV-vis absorption peak (Figure S2 and S3) corresponding to the M direction parallel to the short molecular axis, as reported in the previous study.¹⁷ The computed M in Figure 3 was consistent with the absorption band around 650 nm at 77 K (Figure S2), as explained previously.¹⁸ From the line shape analysis to fit the TREPR spectra of Figure 2a, 2b and 2c, we obtained the principal axis directions of the ZFS interaction of **[28]Hex** for the negative D by using the polar ($\delta = 60^\circ$) and azimuthal ($\gamma = 40^\circ$) angles of M (Figure S6) in the principal XYZ axis system, as shown in Figure 3.

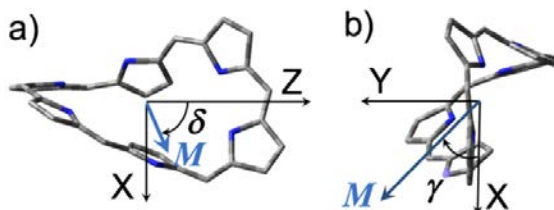


Figure 3. Orientations ($\delta = 60^\circ$ and $\gamma = 40^\circ$) of the principal ZFS principal axes with respect to the transition dipole moment (M) of **[28]Hex** determined by MPS in Figure 2. Views of **[28]Hex** from the Y and the Z axes are shown in a) and in b), respectively.

Together with the MPS effect, the anisotropy in ISC from the lowest excited singlet state (S_1 state) to the triplet spin sublevels allows us to characterize the direction of the Z axis, since such anisotropies are governed by the spin-orbit coupling (SOC) scheme between the singlet and triplet characters.^{42,43} In the case of the negative D , $P_X = 0$, $P_Y = 0.60$ and $P_Z = 0.40$ were obtained to fit the E/A/E/A/E/A polarization pattern, as shown in Figure 4a. The S_1 - T_1 ISC should occur via the $^1n\pi^* \rightarrow ^3\pi'\pi^*$ transition scheme driven by the SOC with borrowing highly

lying $^1n\pi^*$ in the S_1 state of $^1\pi\pi^*$.⁴⁰ We found an n-orbital character of orbital #115 (Figure 4b) by the MO calculation of a **[28]Hex** model molecule with the B3LYP/6-31G* level. In the ZFS principal axes system in Figure 3, the n-orbitals on the nitrogen atoms labeled by “N” in Figure 4b are directing roughly to the Z and X axes and are orthogonal to π orbitals (π' in Figure 4c) at the nitrogen positions. The S_1 - T_n ISC is thus active both to the T_Y and T_Z sublevels (i. e. $P_Y \approx P_Z \gg P_X$) through the SOC during the $^1n\pi^* \rightarrow ^3\pi'\pi^*$ transitions in Figure 4c because of the twisted molecular topology in Figure 4b. This is in line with the anisotropy in the ISC scheme obtained for the negative D in Figure 4a. It is thus concluded that the sign of the D is negative with the principal Z axis directing along with the molecular long axis. This also specifies that the spin-density distribution is not fully delocalized in the **[28]Hex** macrocycle in the T_1 state, as predicted by the MO calculations (Figure S4b). This character is totally different from the delocalized spin distributions in 3 **[26]Hex*** (Figure S4a) and $^3H_2P^*$. Interestingly, this localized character in the T_1 state is also totally different from the delocalized character in the S_1 state¹⁸ of the twisted **[28]Hex**.

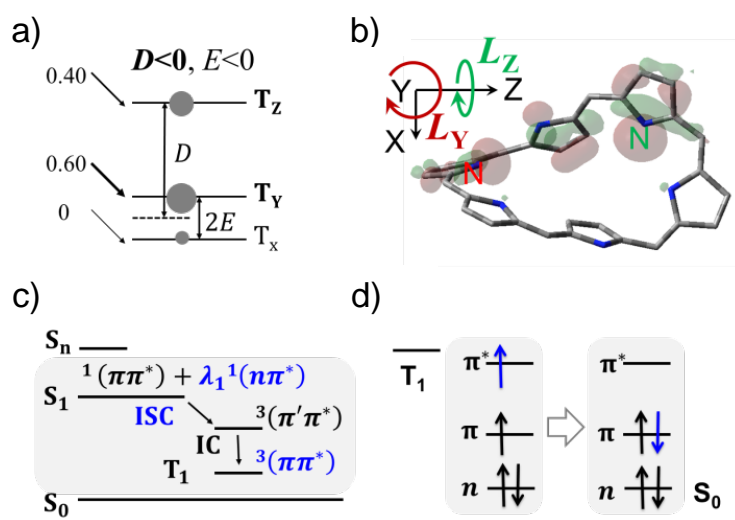


Figure 4. a) Relative populations in the triplet sublevels at 0.5 μs in **[28]Hex**. b) The n-orbital character involving the $^1n\pi^* \rightarrow ^3\pi'\pi^*$ ISC which induces the angular momentum changes along the Y and Z axes. c) Schematic representation of the S_1 - T_1 ISC in **[28]Hex**. d) The deactivation scheme of the T_1 state leading to S_0 , contributing to the anisotropy in the T_1 sublevels to account for the spin polarizations for $t > 5 \mu\text{s}$ in Figure 2.

Further insights into the electronic structure of the T_1 state were obtained by spectrum changes in Figure 2 for $t > 5 \mu\text{s}$. From Figure 2d, 2g, and 2j, the line-shapes were modulated from the E/A/E/A/E/A pattern to A/A/A/E/E/E by the delay time. In a previous study, time-dependent EPR spectra were interpreted in terms of sublevel-dependent depopulations by a triplet-triplet energy-transfer.⁴⁹ In the present case, the A/A/A/E/E/E pattern is explained by a quick T_Z depletion, as shown by Figure 5a. We quantitatively fitted the delay time dependence of the transverse magnetizations in Figure S7 with taking into account the time-dependent sublevel populations determined by depletion rates (k_X , k_Y and k_Z in Figure 5a) from the X, Y and Z sublevels, respectively, as detailed in SI. The deactivation kinetics of $k_T = (k_X + k_Y + k_Z)/3 = 16 \text{ ms}^{-1}$ from Figure 5a is consistent with reported lifetime (90 μs) of $^3\text{[28]Hex}^*$ at 170 K obtained by the transient absorption spectroscopy.²⁷

The deactivation of the triplet CT character $^3(D^{+\bullet}-A^{-\bullet})$ as shown by Figure 4d leads to the electron spin polarization in the triplet state. Figure 5b and Figure 5c show views of the orbitals of π (orbital number = 122 α) and π^* (123 α) from the Y and Z axes, respectively, obtained by the DFT calculation of the T_1 state of the **[28]Hex** model molecule. Taking these CT unpaired orbitals as a configuration contributing to the T_1 state, the two spins are separated from each

other as shown in Figure 5b. Thanks to the twisted molecular topology in the [28]Hex framework, the π^* orbital possesses the atomic orbital contribution which is orthogonal to the atomic orbital participating in the π orbital. These atomic orbital contributions in π^* and π are

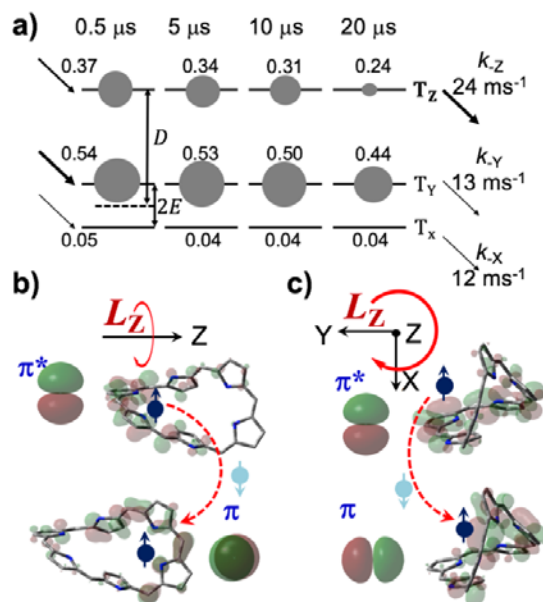


Figure 5. a) Relative populations in the zero-field triplet sublevels obtained for $D < 0$ and $E < 0$ of [28]Hex at several delay times to account for the spin polarization changes. b), c) The CT character is represented by the orbitals of π (orbital number = 122α) and π^* (123α) obtained by the DFT calculation. The twisted molecules are viewed from the Y and Z axes in b) and c), respectively. Representative topologies of the localized unpaired orbitals are depicted by the p-orbitals in b) and c), demonstrating that the SOC is effective as the angular momentum change (L_z) along the Z axis to cause the spin-flip (dotted arrows) for the T_z depopulation during the $\pi\pi^* \rightarrow \pi^2$ transition.

represented by the p_x and p_y orbitals, respectively in Figure 5b and Figure 5c. Therefore, the angular momentum change is effective along the Z axis during the $\pi^* \rightarrow \pi$ transition in the reverse ISC from $^3\pi\pi^*$ to $^1\pi^2$, since the rotation (L_z) of the p_x orbital results in the p_y orbital as shown by the dotted arrows in Figure 5b and Figure 5c. The T_z depletion caused by the spin flip is thus interpreted by the effective SOC described by the matrix element of $\langle ^1(D-A) | \mathbf{H}_{\text{SOC}} | ^3(D^{+\bullet}-A^{-\bullet}) \rangle$ in the T_z sublevel. The above SOC-induced depopulation scheme is relevant to an ISC mechanism in which the SOC is operative during the triplet charge-recombination between the orthogonal unpaired orbitals of $D^{+\bullet}$ and $A^{-\bullet}$ in the singlet CT state of donor (D) – acceptor (A) linked molecules (D-A), generating the locally excited triplet state, i.e. $^1(D^{+\bullet}-A^{-\bullet}) \rightarrow (D^{-3}A^*)$, as reported by Wasielewski.⁵⁰ The present T_z depopulation thus denotes that the intramolecular CT character is involved in the T_1 state of the twisted **[28]Hex**. This well explains CT:LE = 1:5 obtained from the CI coefficients in the triplet state, as described above. We also calculated the D value ($D^{\text{SS}} = -746$ MHz as the spin-spin contribution) from the unpaired orbital distributions in Figure S4b obtained by the CIS method.^{35,51-53} The details on the calculations are described in section 1-4 of SI. The relation of $D^{\text{SS}} = 1.4 D$ agrees with the correlations between the computed D^{SS} and the D values (Table S1) obtained for tetraphenylporphyrins and hexaphyrins, supporting the coexistence of the LE and CT characters in the twisted **[28]Hex**.

Since the electronic characters in the T_1 states of the planar **[26]Hex** and the twisted **[28]Hex** are well compatible with the theoretical calculations (Table S1), one may evaluate the antiaromatic/aromatic characters of the T_1 states both in **[26]Hex** and **[28]Hex** on the basis of the DFT calculations. (Table S2 and S3) The validity of utilizing the (U)B3LYP levels of theory^{54,55} in the model molecules is detailed in section 1-4 and in Table S3 of SI. The NICS(0) of the twisted Möbius **[28]Hex** exhibited a large positive NICS(0) of 60 ppm in the T_1 state. This is in

contrast to the negative NICS(0) of -15 ppm in the S_0 state in Table S2, demonstrating the reversal relationship between the aromaticity and the antiaromaticity in the S_0 and T_1 states, respectively. We also computed the state energies (Table S3) of the S_0 and T_1 states using the DFT calculations for the planar **[26]Hex**, the planar **[28]Hex** and the twisted **[28]Hex**. In planar **[28]Hex**, which is a conformational isomer of twisted **[28]Hex**, the T_1 - S_0 energy gap of $\Delta E(T_1-S_0)$ was significantly smaller (0.29 eV) than the corresponding gap (1.10 eV) in the twisted **[28]Hex** in Table S3. This is explained by the aromatic character in the T_1 state of the planar **[28]Hex** since the energy difference (0.1 eV) is very small between the S_0 states of the planar and twisted **[28]Hex** molecules²⁷; the T_1 is highly stable in the planar **[28]Hex** due to the aromaticity in the excited state as the reversal to the Hückel $[4n]$ antiaromaticity in S_0 according to the Baird's rule, as confirmed by the negative NICS(0) value of -17 ppm in the T_1 state (Table S2). On the ground-state aromaticity molecules of **[26]Hex** and twisted **[28]Hex**, $\Delta E(T_1-S_0) = 1.10$ eV was slightly larger in the twisted **[28]Hex** than that (0.95 eV) in **[26]Hex**. This higher T_1 energy in the twisted 3 **[28]Hex*** should not be associated with the LE character as described in section 1-4 of SI because the delocalized distribution leads to the electronic destabilization in the antiaromatic state due to the positive resonance energy³² for the extended π -conjugation systems in 3 **[26]Hex*** (Figure S4a). Alternatively, the triplet CT character in 3 **[28]Hex*** would cause the electronic destabilization by a weakened spin-spin exchange interaction between the separated unpaired orbitals in Figure 5b.

In conclusion, we have revealed the electronic structure of the T_1 state of **[28]Hex** by using the TREPR method in combination with the MO calculations as the first example of twisted Möbius aromatic molecules. The contribution of the intramolecular CT character together with the LE character at one side in the Möbius strip ring of the macrocycle has been demonstrated. The lack

of the spin-spin exchange stabilization between the separated unpaired electrons causes the destabilized triplet state, resulting in antiaromaticity. Besides the energetics and the ring current effects that are used to evaluate the aromaticity/antiaromaticity, the quick SOC-induced triplet deactivation faster than $k_T = 10^4 \text{ s}^{-1}$ (Figure 5a) can be an alternate important barometer to represent the “antiaromaticity” because of the connection between the orthogonal CT character and the triplet instability. It is noted that k_T is usually smaller than 10^4 s^{-1} in the $^3\pi\pi^*$ of the planar metal-free Hückel aromatic molecules at cryogenic temperatures for $\Delta E(T_1-S_0) \approx 1 \text{ eV}$,^{56,57} highlighting the remarkably accelerated deactivation by the orthogonal $^3\pi\pi^*$ (Figure 5b) in the antiaromatic T_1 state. The present relationship between the aromaticity/antiaromaticity and the electronic structures is highly informative for understanding the fundamental chemical reactivity of Möbius aromatic molecules for future designs of the functional organic molecules.

ASSOCIATED CONTENT

Supporting Information. This file is available free of charge. Experimental methods, TREPR spectra of [26]Hex, UV-vis absorption spectra, gross spin density distributions, molecular orbitals, line shape analyses of the TREPR spectra, ZFS parameters, NICS values, calculated state energies, cartesian coordinates of optimized geometries are described. (PDF)

AUTHOR INFORMATION

Notes

The authors declare no competing financial interests.

ACKNOWLEDGMENT

The work at Kobe University was supported by a Grant-in-Aid for Scientific Research (Nos. 17K19105 and 16H04097 to Y. Kobori) from the Ministry of Education, Culture, Sports, Science and Technology, Japan. The work at Kyoto University was supported by Grants-in-Aid from JSPS (Nos.: 25220802 and 16K13952 to A. Osuka). The group of Osaka City University (OCU) acknowledged support from the AOARD Scientific Project on “Quantum Properties of Molecular Nanomagnets” (Award No. FA2386-13-4029, 13-4030, 13-4031) and AOARD Project on “Molecular Spins for Quantum Technologies” (Grant No. FA2386-17-1-4040). The OCU group acknowledged partial support by Grants-in-Aid for Scientific Research on Innovative Areas (Quantum Cybernetics) from the MEXT and by the FIRST Quantum Information Processing Project, the Cabinet Office (Japan).

REFERENCES

- (1) Rosenberg, M.; Dahlstrand, C.; Kilsa, K.; Ottosson, H., Excited State Aromaticity and Antiaromaticity: Opportunities for Photophysical and Photochemical Rationalizations. *Chem. Rev.* **2014**, *114*, 5379-5425.
- (2) Merino, G.; Heine, T.; Seifert, G., The Induced Magnetic Field in Cyclic Molecules. *Chem. Eur. J.* **2004**, *10*, 4367-4371.
- (3) Gomes, J.; Mallion, R., Aromaticity and Ring Currents. *Chem. Rev.* **2001**, *101*, 1349-1384.
- (4) Schleyer, P. v. R.; Maerker, C.; Dransfeld, A.; Jiao, H.; van Eikema Hommes, N. J., Nucleus-Independent Chemical Shifts: a Simple and Efficient Aromaticity Probe. *J. Am. Chem. Soc.* **1996**, *118*, 6317-6318.
- (5) von Schleyer, P. R.; Jiao, H., What is Aromaticity? *Pure Appl. Chem.* **1996**, *68*, 209-218.
- (6) Kruszewski, J.; Krygowski, T., Definition of Aromaticity Basing on the Harmonic Oscillator Model. *Tetrahedron Lett.* **1972**, *13*, 3839-3842.

- (7) Aihara, J.-I., Circuit Resonance Energy: A Key Quantity That Links Energetic and Magnetic Criteria of Aromaticity. *J. Am. Chem. Soc.* **2006**, *128*, 2873-2879.
- (8) Cyrański, M. K., Energetic Aspects of Cyclic π -Electron Delocalization: Evaluation of the Methods of Estimating Aromatic Stabilization Energies. *Chem. Rev.* **2005**, *105*, 3773-3811.
- (9) Möbius, K., Plato, M., Klihm, G., Laurich, C., Savitsky, A., Lubitz, W., Szyszko, B., Stepień, M., Latos-Grazynski, L., Möbius–Hückel Topology Switching in an Expanded Porphyrin Cation Radical as Studied by EPR and ENDOR Spectroscopy. *Phys. Chem. Chem. Phys.* **2015**, *17*, 6644-6652.
- (10) Hückel, E., Quantentheoretische Beiträge zum Benzolproblem. *Zeitschrift für Physik* **1931**, *70*, 204-286.
- (11) Heilbronner, E., Hückel Molecular Orbitals of Möbius-type Conformations of Annulenes. *Tetrahedron Lett.* **1964**, *5*, 1923-1928.
- (12) Krygowski, T. M.; Cyrański, M., Separation of the Energetic and Geometric Contributions to the Aromaticity of π -Electron Carbocyclics. *Tetrahedron* **1996**, *52*, 1713-1722.
- (13) Schaller, G. R.; Topić, F.; Rissanen, K.; Okamoto, Y.; Shen, J.; Herges, R., Design and Synthesis of the First Triply Twisted Möbius Annulene. *Nat. Chem.* **2014**, *6*, 608-613.
- (14) Stepień, M.; Latos-Grażyński, L.; Sprutta, N.; Chwalisz, P.; Szterenber, L., Expanded Porphyrin with a Split Personality: A Hückel–Möbius Aromaticity Switch. *Angew. Chem. Int. Ed.* **2007**, *46*, 7869-7873.
- (15) Tanaka, Y.; Saito, S.; Mori, S.; Aratani, N.; Shinokubo, H.; Shibata, N.; Higuchi, Y.; Yoon, Z. S.; Kim, K. S.; Noh, S. B., Metalation of Expanded Porphyrins: a Chemical Trigger Used to Produce Molecular Twisting and Möbius Aromaticity. *Angew. Chem. Int. Ed.* **2008**, *47*, 681-684.

- (16) Jux, N., The Porphyrin Twist: Hückel and Möbius Aromaticity. *Angew. Chem. Int. Ed.* **2008**, *47*, 2543-2546.
- (17) Osuka, A.; Saito, S., Expanded Porphyrins and Aromaticity. *Chem. Commun.* **2011**, *47*, 4330-4339.
- (18) Sankar, J.; Mori, S.; Saito, S.; Rath, H.; Suzuki, M.; Inokuma, Y.; Shinokubo, H.; Suk Kim, K.; Yoon, Z. S.; Shin, J.-Y., Unambiguous Identification of Möbius Aromaticity for meso-Aryl-substituted [28] hexaphyrins (1.1. 1.1. 1.1). *J. Am. Chem. Soc.* **2008**, *130*, 13568-13579.
- (19) Ottosson, H.; Borbas, K. E., Aromaticity: A Light-Switched Yin and Yang pair. *Nat. Chem.* **2015**, *7*, 373.
- (20) Sung, Y.; Yoon, M.; Lim, J.; Rath, H.; Naoda, K.; Osuka, A.; Kim, D., Reversal of Hückel (Anti) Aromaticity in the Lowest Triplet States of Hexaphyrins and Spectroscopic Evidence for Baird's rule. *Nat. Chem.* **2015**, *7*, 418-422.
- (21) Yoon, Z. S.; Osuka, A.; Kim, D., Möbius Aromaticity and Antiaromaticity in Expanded Porphyrins. *Nat. Chem.* **2009**, *1*, 113-122.
- (22) Shin, J.-Y.; Furuta, H.; Yoza, K.; Igarashi, S.; Osuka, A., meso-Aryl-Substituted Expanded Porphyrins. *J. Am. Chem. Soc.* **2001**, *123*, 7190-7191.
- (23) Saito, S.; Osuka, A., Expanded Porphyrins: Intriguing Structures, Electronic Properties, and Reactivities. *Angew. Chem. Int. Ed.* **2011**, *50*, 4342-4373.
- (24) Misra, R.; Chandrashekar, T. K., Structural Diversity in Expanded Porphyrins. *Acc. Chem. Res.* **2008**, *41*, 265-279.
- (25) Shimizu, S.; Osuka, A., Metalation Chemistry of meso-Aryl-Substituted Expanded Porphyrins. *Eur. J. Inorg. Chem.* **2006**, *2006*, 1319-1335.
- (26) Lim, J. M.; Yoon, Z. S.; Shin, J.-Y.; Kim, K. S.; Yoon, M.-C.; Kim, D., The Photophysical Properties of Expanded Porphyrins: Relationships between Aromaticity,

Molecular Geometry and Non-linear Optical Properties. *Chem. Commun.* **2009**, *45*, 261-273.

- (27) Kim, K. S.; Yoon, Z. S.; Ricks, A. B.; Shin, J.-Y.; Mori, S.; Sankar, J.; Saito, S.; Jung, Y. M.; Wasielewski, M. R.; Osuka, A., Temperature-Dependent Conformational Change of meso-Hexakis (pentafluorophenyl)[28] Hexaphyrins (1.1. 1.1. 1.1) into Mobius Structures. *J. Phys. Chem. A* **2009**, *113*, 4498-4506.
- (28) Ahn, T. K.; Kwon, J. H.; Kim, D. Y.; Cho, D. W.; Jeong, D. H.; Kim, S. K.; Suzuki, M.; Shimizu, S.; Osuka, A.; Kim, D., Comparative Photophysics of [26]-and [28] Hexaphyrins (1.1. 1.1. 1.1): Large Two-Photon Absorption Cross Section of Aromatic [26] Hexaphyrins (1.1. 1.1. 1.1). *J. Am. Chem. Soc.* **2005**, *127*, 12856-12861.
- (29) Oh, J.; Sung, Y. M.; Kim, W.; Mori, S.; Osuka, A.; Kim, D., Aromaticity Reversal in the Lowest Excited Triplet State of Archetypical Möbius Heteroannulenic Systems. *Angew. Chem. Int. Ed.* **2016**, *55*, 6487-6491.
- (30) Sung, Y. M.; Oh, J.; Kim, W.; Mori, H.; Osuka, A.; Kim, D., Switching between Aromatic and Antiaromatic 1, 3-phenylene-strapped [26]-and [28] Hexaphyrins upon Passage to the Singlet Excited State. *J. Am. Chem. Soc.* **2015**, *137*, 11856-11859.
- (31) Ottosson, H., Organic Photochemistry: Exciting Excited-State Aromaticity. *Nat. Chem.* **2012**, *4*, 969-971.
- (32) Aihara, J.-I., Resonance Energies of Annulenes and Radialenes. *Bull. Chem. Soc. Jpn.* **1975**, *48*, 517-520.
- (33) Aihara, J.-I., Aromaticity-Based Theory of Pericyclic Reactions. *Bull. Chem. Soc. Jpn.* **1978**, *51*, 1788-1792.
- (34) Baird, N. C., Quantum Organic Photochemistry. II. Resonance and Aromaticity in the Lowest $^3\pi\pi^*$ State of Cyclic Hydrocarbons. *J. Am. Chem. Soc.* **1972**, *94*, 4941-4948.
- (35) Tanabe, M.; Matsuoka, H.; Ohba, Y.; Yamauchi, S.; Sugisaki, K.; Toyota, K.; Sato, K.; Takui, T.; Goldberg, I.; Saltsman, I., Time-Resolved Electron Paramagnetic

- Resonance and Phosphorescence Studies of the Lowest Excited Triplet States of Rh (III) Corrole Complexes. *J. Phys. Chem. A* **2012**, *116*, 9662-9673.
- (36) Yamauchi, S.; Takahashi, K.; Islam, S. S.; Ohba, Y.; Tarasov, V., Time-Resolved High-Frequency EPR Studies on Magnesium and Zinc Tetraphenylporphines in their Lowest Excited Triplet States. *J. Phys. Chem. B* **2010**, *114*, 14559-14563.
- (37) McGlynn, S. P.; Azumi, T.; Kinoshita, M., *Molecular spectroscopy of the triplet state*. Prentice Hall: New Jersey, **1969**.
- (38) Gonen, O.; Levanon, H., Line-Shape Analysis of Transient Triplet Electron Paramagnetic Resonance Spectra. Application to Porphyrins and Chlorophylls in Nematic Uniaxial Liquid Crystals. *J. Phys. Chem.* **1984**, *88*, 4223-4228.
- (39) Murai, H.; Imamura, T.; Obi, K., Time-Resolved ESR Detection of Benzophenone $n\pi^*$ Triplet State in Glassy Matrices at 77 K. *Chem. Phys. Lett.* **1982**, *87*, 295-298.
- (40) Tait, C. E.; Neuhaus, P.; Peeks, M. D.; Anderson, H. L.; Timmel, C. R., Transient EPR Reveals Triplet State Delocalization in a Series of Cyclic and Linear π -Conjugated Porphyrin Oligomers. *J. Am. Chem. Soc.* **2015**, *137*, 8284-8293.
- (41) Di Valentin, M.; Biasibetti, F.; Ceola, S.; Carbonera, D., Identification of the Sites of Chlorophyll Triplet Quenching in Relation to the Structure of LHC-II from Higher Plants. Evidence from EPR Spectroscopy. *J. Phys. Chem. B* **2009**, *113*, 13071-13078.
- (42) Tait, C. E.; Neuhaus, P.; Anderson, H. L.; Timmel, C. R., Triplet State Delocalization in a Conjugated Porphyrin Dimer Probed by Transient Electron Paramagnetic Resonance Techniques. *J. Am. Chem. Soc.* **2015**, *137*, 6670-6679.
- (43) Michaeli, S.; Soffer, S.; Levanon, H.; Senge, M. O.; Kalisch, W. W., Triplet Dynamics of Conformationally Distorted Porphyrins in Isotropic Liquids and Liquid Crystals. Time-Resolved Electron Paramagnetic Resonance Study. *J. Phys. Chem. A* **1999**, *103*, 1950-1957.

- (44) Salvadori, E.; Di Valentin, M.; Kay, C. W.; Pedone, A.; Barone, V.; Carbonera, D., The Electronic Structure of the Lutein Triplet State in Plant Light-Harvesting Complex II. *Phys. Chem. Chem. Phys.* **2012**, *14*, 12238-12251.
- (45) Borovykh, I. V.; Klenina, I. B.; Proskuryakov, I. I.; Gast, P.; Hoff, A. J., Magnetophotoselection Study of the Carotenoid Triplet state in *Rhodobacter Sphaeroides* Reaction Centers. *J. Phys. Chem. B* **2002**, *106*, 4305-4312.
- (46) Frank, H. A.; Bolt, J.; Friesner, R.; Sauer, K., Magnetophotoselection of the Triplet State of Reaction Centers from *Rhodospseudomonas Sphaeroides* R-26. *Biochim. Biophys. Acta-Bioenergetics* **1979**, *547*, 502-511.
- (47) Thurnauer, M. C.; Norris, J. R., The Ordering of the Zero Field Triplet Spin Sublevels in the Chlorophylls. A Magnetophotoselection Study. *Chem. Phys. Lett.* **1977**, *47*, 100-105.
- (48) Borovykh, I. V.; Proskuryakov, I. I.; Klenina, I. B.; Gast, P.; Hoff, A. J., Magnetophotoselection Study of the Lowest Excited Triplet State of the Primary Donor in Photosynthetic Bacteria. *J. Phys. Chem. B* **2000**, *104*, 4222-4228.
- (49) Di Valentin, M.; Tait, C.; Salvadori, E.; Ceola, S.; Scheer, H.; Hiller, R. G.; Carbonera, D., Conservation of Spin Polarization during Triplet–Triplet Energy Transfer in Reconstituted Peridinin–Chlorophyll–Protein Complexes. *J. Phys. Chem. B* **2011**, *115*, 13371-13380.
- (50) Wasielewski, M. R.; Johnson, D. G.; Svec, W. A.; Kersey, K. M.; Minsek, D. W., Achieving High Quantum Yield Charge Separation in Porphyrin-Containing Donor-Acceptor Molecules at 10 K. *J. Am. Chem. Soc.* **1988**, *110*, 7219-7221.
- (51) Yamauchi, S.; Tanabe, M.; Ohba, Y.; Sugisaki, K.; Toyota, K.; Sato, K.; Takui, T.; Saltsman, I., Complete Assignment of Spin Sublevels in the Lowest Excited Triplet State of Corrole Compounds by Time-Resolved EPR Spectroscopy. *Chem. Phys. Lett.* **2012**, *521*, 64-68.

- (52) McWeeny, R.; Mizuno, Y. In *The Density Matrix in Many-Electron Quantum Mechanics II. Separation of Space and Spin Variables; Spin Coupling Problems*, Proc. R. Soc. Lond. A, The Royal Society: **1961**, 554-577.
- (53) Sugisaki, K.; Toyota, K.; Sato, K.; Shiomi, D.; Kitagawa, M.; Takui, T., Ab initio Calculations of Spin–Orbit Contribution to the Zero-Field Splitting Tensors of $n\pi^*$ Excited States by the CASSCF Method with MRMP2 Energy Correction. *Chem. Phys. Lett.* **2009**, *477*, 369-373.
- (54) Marcos, E.; Anglada, J. M.; Torrent-Sucarrat, M. Theoretical Study of the Switching between Hückel and Möbius Topologies for Expanded Porphyrins. *J. Phys. Chem. C* **2012**, *116*, 24358-24366.
- (55) Torrent-Sucarrat, M.; Navarro, S.; Cossio, F. P.; Anglada, J. M.; Luis, J. M. Relevance of the DFT Method to Study Expanded Porphyrins with Different Topologies. *J. Comput. Chem.* **2017**, *38*, 2819-2828.
- (56) Matsuoka, H.; Retegan, M.; Schmitt, L.; Höger, S.; Neese, F.; Schiemann, O., Time-Resolved Electron Paramagnetic Resonance and Theoretical Investigations of Metal-Free Room-Temperature Triplet Emitters. *J. Am. Chem. Soc.* **2017**, *139*, 12968-12975.
- (57) Gouterman, M.; Khalil, G.-E., Porphyrin Free Base Phosphorescence. *J. Mol. Spectroscopy* **1974**, *53*, 88-100.

Supporting Information of

Charge-Transfer Character Drives Möbius
Antiaromaticity in the Excited Triplet State of
Twisted [28]Hexaphyrin

Fumitoshi Ema,[†] Mana Tanabe,^{§,£} Shohei Saito,[‡] Tomoki Yoneda,^{‡,£} Kenji Sugisaki,[¶] Takashi Tachikawa,^{†,£} Seiji Akimoto,[†] Seigo Yamauchi,^{§,#} Kazunobu Sato,^{,¶} Atsuhiko Osuka,^{*,‡} Takeji Takui,^{*,¶} and Yasuhiro Kobori^{*,†,£}.*

[†]Department of Chemistry, Graduate School of Science, Kobe University, 1-1 Rokkodai-cho, Nada-ku, Kobe 657-8501, Japan

[§]Institute of Multidisciplinary Research for Advanced Materials, Tohoku University, Katahira 2-1-1, Aoba-ku, Sendai 980-8577, Japan

[‡]Department of Chemistry, Graduate School of Science, Kyoto University, Sakyo-ku, Kyoto 606-8502, Japan

[¶]Department of Chemistry and Molecular Materials Science, Graduate School of Science, Osaka City University, 3-3-138 Sugimoto, Sumiyoshi-ku, Osaka 558-8585, Japan

[£]Molecular Photoscience Research Center, Kobe University, 1-1 Rokkodai-cho, Nada-ku, Kobe 657-8501, Japan

Table of Contents

1. Experimental Procedures	
1-1. Materials and Sample Preparations	S2
1-2. UV-Vis Absorption Measurements	S3
1-3. TREPR Measurements	S3
1-4. Theoretical Calculations	S3
2. TREPR Spectra of [26]Hex	S6
3. UV-Vis Absorption Spectra	S6
4. Gross spin density distribution	S8
5. Molecular Orbitals	S8
6. Line Shape Analyses of the TREPR Spectra	S9
7. ZFS Parameters	S13
8. NICS Values	S14
9. Calculated state energies	S14
10. Cartesian Coordinates of Optimized Geometries	S15

Experimental Procedures

1-1. Materials and Sample Preparations

The details in synthesis process of *meso*-hexakis(pentafluorophenyl) [26]Hexaphyrins(1.1.1.1.1.1) and *meso*-hexakis(pentafluorophenyl) [28]Hexaphyrins(1.1.1.1.1.1) ([26]Hex and [28]Hex) are described in the previous reports.¹ Toluene (JIS Special Grade) and 2-methyltetrahydrofuran (MTHF, Wako Special Grade) were purchased from Wako Pure Chemical Industries, Ltd., and they were used as received. For UV-vis absorption and time-resolved EPR (TR-EPR) measurements, [26]Hex and [28]Hex were dissolved in toluene and MTHF, respectively. The concentrations of these solutions were 100-200 μ M. For the TR-EPR measurements, in addition, these solutions were

deoxygenated by the freeze-pump-thaw cycle and were sealed in quartz EPR sample tubes before the X-band TR-EPR measurements.

1-2. UV-vis absorption measurements

UV-vis absorption spectra at room temperature were measured on a SHIMAZDU UV-1650PC spectrometer with a 0.1 cm optical path length quartz cell. UV-vis absorption spectra at 77 K were measured on a JASCO V-650 equipped with an integrating sphere unit ISVC-747, where the sample tube including sample solution was set into a Dewar bottle filled with liquid nitrogen.

1-3. Time-resolved EPR measurements

Time-resolved EPR (TREPR) spectra were measured using a Bruker EMX X-band continuous wave (CW) EPR spectrometer without magnetic field modulation at 77 K. The EPR sample tubes were placed in a Dewar bottle filled with liquid nitrogen, which was set inside the EPR cavity. A nanosecond-pulsed OPO laser (Spectra-Physics, basiscan/L13P-KE; $\lambda = 568$ nm and 650 nm, 10 Hz) pumped by a pulsed Nd:YAG laser (Spectra-Physics, Quanta-Ray Lab-130; $\lambda = 355$ nm) was used as an excitation light as reported in our previous study. Details of the detection method were given previously.² Microwave power was set to be 4-5 mW. A quartz depolarizer (Sigmakoki, DEQ-1N) was employed for depolarized laser excitations. A quartz $\lambda/2$ waveplate (Sigmakoki, WPQW-65/78-2M) was used for introducing the polarized light converting the direction of polarization in 90 degrees. In magnetophotoselection (MPS) experiments, the polarization directions of the laser (L) were set parallel ($B_0 // L$) and perpendicular ($B_0 \perp L$) to the direction of the external magnetic field (B_0). In the MPS measurements, the excitation wavelengths were selected as described in [Figure S2](#) and [S3](#).

1-4. Theoretical Calculations

Geometry optimizations of the ground state of [26]Hex and [28]Hex were performed by using the density functional theory (DFT) method with the Becke's three parameter hybrid exchange functional and the Lee-Yang-Parr correlation functional (B3LYP)³ with 6-31G* and

6-31G** basis sets⁴ in Gaussian 03⁵ and Gaussian 09 program package.⁶ The Cartesian coordinates of the optimized geometries are listed in [section 10](#) of the present Supporting Information. The pentafluorophenyl groups of **[26]Hex** and **[28]Hex** were replaced with hydrogen atoms. The excitation energy and the oscillator strength calculations were carried out using the ZINDO/S method^{7, 8} in ORCA 3.0.3 program package⁹ and the ZINDO method⁷ in Gaussian 09 program package for the B3LYP/6-31G** optimized geometry. The configuration interaction singles (CIS) calculations¹⁰ were performed by using the restricted Hartree–Fock (RHF) method with a cc-pVDZ basis set¹¹ in Gaussian 03 program package for the B3LYP/6-31G* optimized geometry. The calculations of the zero-field splitting (ZFS) tensors were carried out with Gaussian 03 program suite. The spin–spin contributions (D^{SS} and E^{SS}) to the ZFS parameters were estimated by the McWeeny–Mizuno equation^{12, 13} with CIS/cc-pVDZ spin-densities at the B3LYP/6-31G* optimized geometries. The two-electron dipole–dipole integrals were calculated by using our own codes.¹³ We have noted that the CIS spin density-based approach has a tendency to overestimate the D value for an extended π conjugated system. The CIS calculations, nevertheless, deserved important consideration in determining the sign of the D value and the principal axes orientations of the \mathbf{D} tensor of the systems under study, as shown in Figure 1 in the main text.¹⁴

The NICS values were computed by the gauge including atomic orbital (GIAO) method¹⁵ at the B3LYP/6-31G** level for the S_0 state or at the UB3LYP/6-31G** level for the T_1 state based on the optimized geometries. The NICS values were calculated for the centers of the hexaphyrin macrocycles with zero height as NICS(0) values, as given in the previous reports.^{16, 17}

The T_1 - S_0 energy gaps were obtained as follows. We performed the geometry optimizations for the S_0 state using RB3LYP/6-31G**. For the optimized geometries, we performed the single point energy calculations for the triplet states by using UB3LYP/6-31G**. We also carried out the geometry optimization for the twisted **[28]Hex** model molecule as the triplet state. However, the optimized geometry represented a planer conformation which is categorized as the planar **[28]Hex**. Thus, we did not adopt the optimized geometries for the excited states, since the structure in the T_1 state is frozen as described in the main text. The SCF energy difference between these states are listed in [Table S3](#).

The conformational preference of the twisted **[28]Hex** in the S_0 state was obtained by the RB3LYP/6-31G** calculations as shown in Table S3. It is known that the basis function does not largely influence the state energies but the level of theory does. This preference is probably an accidental coincidence with the predominance of the twisted conformer at lower

temperature, since the theoretical calculations were performed for the model molecules of the hexaphyrins in which the pentafluorophenyl groups were replaced by the hydrogen atoms. It is known that the B3LYP theory exaggerates the delocalization of conjugated systems, overstabilizing the Möbius structures. (Ref.54 in the main text) However, the lack of the pentafluorophenyl groups in the B3LYP/6-31G** calculations seems to compensate for this overstabilization, giving rise to the preference of the twisted structure, while the other method of M05-2X is reported to result in the energetic preference of the Hückel structure for the **[28]Hex** model without the pentafluorophenyl substituents as in Ref. 54 in the main text. From the above argument, the S_0 state energies in Table S3 seem to be appropriate for the aromaticity molecules of **[28]Hex** and **[26]Hex** in Figure 1. As for the T_1 states, such overstabilization effect will not occur in the aromaticity molecules because of the positive resonance energy in the antiaromatic π -conjugation system. Since the localized spin density distribution has been obtained in the T_1 state of the twisted **[28]Hex** model, the delocalization effect should be minor in the T_1 state energy. We have performed the T_1 state calculation utilizing UM05-2X/6-31G* in the twisted **[28]Hex** model molecule for the optimized geometry by M05-2X/6-31G* in the S_0 state. The spin density distribution has been revealed to be slightly more delocalized than the distribution obtained by the UB3LYP/6-31G*. The computed D value of $D(\text{M05-2X}) = -763$ MHz is almost identical with $D(\text{B3LYP}) = -746$ MHz obtained from the UB3LYP/6-31G* level, denoting that the electronic structure is unaffected by the level of theory. The vertical T_1 - S_0 energy gap has been obtained to be 1.21 eV by the UM05-2X/6-31G*. This energy is slightly higher than 1.10 eV in Table S3. These results indicate that the localized spin density distribution lowers the T_1 state energy which is rationalized by the stronger spin-spin exchange coupling in the excited triplet state. It is noted here that even when the spin density distribution is more localized in the UB3LYP/6-31G* calculation for the twisted **[28]Hex** model, the T_1 state energy is still larger than that in the planar **[26]Hex** model where spin density distribution is highly delocalized. This higher T_1 level would be thus explained by the weakened exchange integral by the involvement of the intramolecular CT character, as described in the main text.

Results and Discussion

2. TREPR spectra of [26]Hex

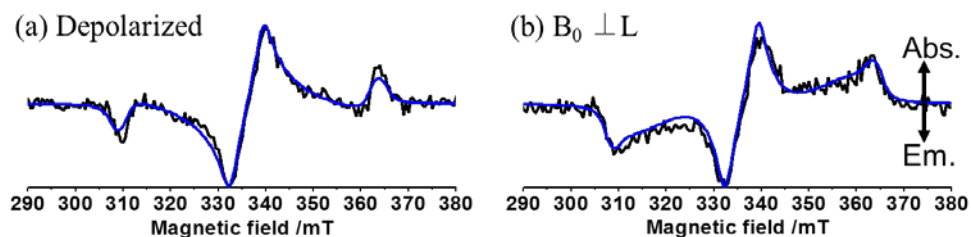
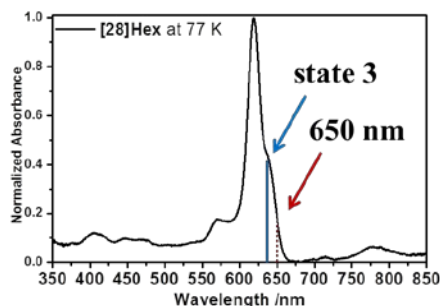


Figure S1. Experimental TREPR spectra of [26]Hex observed in MTHF at 0.5 μ s after 568 nm laser irradiation at 77 K. The depolarized and $B_0 \perp L$ spectra were obtained when the polarization direction of the laser light (L) was depolarized and perpendicular to the external magnetic field (B_0), respectively. Black and blue lines are the experimental and simulated spectra, respectively.

3. UV-Vis Absorption Spectra

In the absorption spectra of [28]Hex observed at 77 K (Figure S2) the strong absorption peak is obtained at 619 nm. Also, the shoulder band around 640 nm is observed. These absorption bands correspond to the transition moments along the long and short molecular axes in the twisted Möbius [28]Hex, on the basis of the calculated absorption spectrum (ref¹⁶ and Figure S3) obtained by the ZINDO method. Thus, 650 nm excitation wavelength as pointed in Figure S2 was used to excite the transition dipole moment along the short molecular axis.



This will avoid the excitation of the other transition dipole moments around 620 nm. A different MPS effect was obtained when 598 nm laser light was chosen, since this light corresponds to the long-axis excitation.

Figure S2. UV-vis absorption spectrum of [28]Hex in toluene at 77 K. A peak shown by state 3 at 630 nm corresponds to the transition dipole moment along the short molecular axis. This assignment

of the direction of the dipole moment was supported by the theoretical calculation by the ZINDO method in [Figure S3](#)

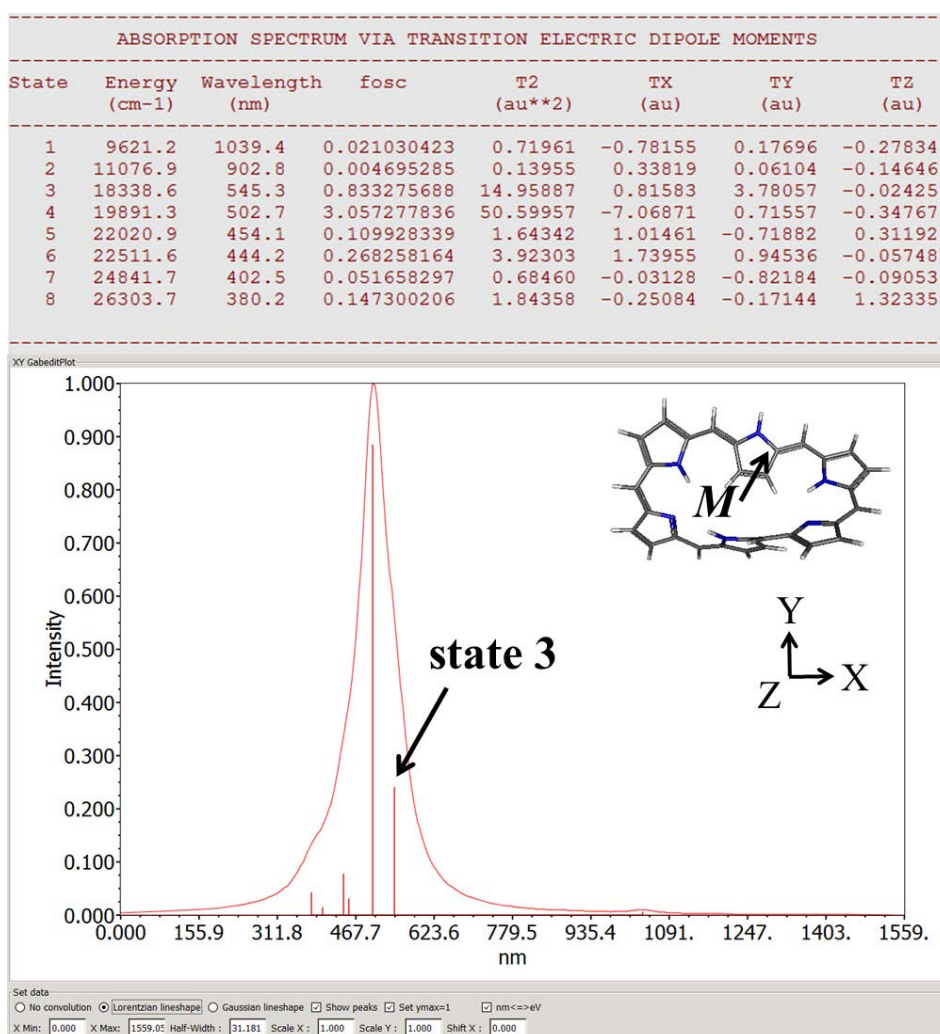


Figure S3. Calculated absorption spectrum and oscillator strength of twisted Möbius **[28]Hex** whose pentafluorophenyl groups are replaced with hydrogen atoms using the ZINDO/S method for the B3LYP/6-31G** optimized geometry. The inset shows the B3LYP/6-31G** optimized geometry and the molecular axes to express the directions of the transition dipole moment. The state 3 (545 nm band as denoted by the arrow) corresponds to the shoulder absorption band at 650 nm indicated by the arrow in [Figure S2](#). The large transition intensity at TY in the state 3 is compatible with the direction of *M* depicted in [Figure 3](#) in the main text.

4. Gross spin density distributions

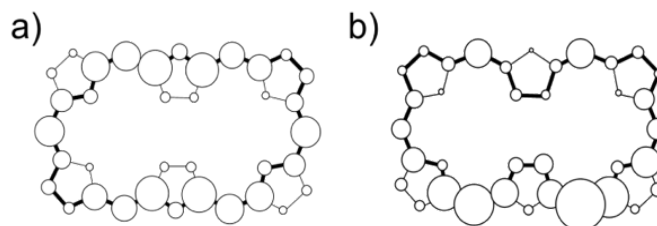


Figure S4. Gross spin density distributions of (a) planar **[26]Hex** and (b) twisted Möbius **[28]Hex** whose pentafluorophenyl groups are replaced with hydrogen atoms. The CIS/cc-pVDZ level was employed for the B3LYP/6-31G* optimized geometry in the ground state.

5. Molecular Orbitals

Excited State 1: Triplet-A
0.5932 eV 2090.25 nm f=0.0000

119 ->125	0.11875
120 ->126	-0.12515
121 ->123	-0.21174
121 ->124	-0.33737
122 ->123	0.48908
122 ->124	-0.10656

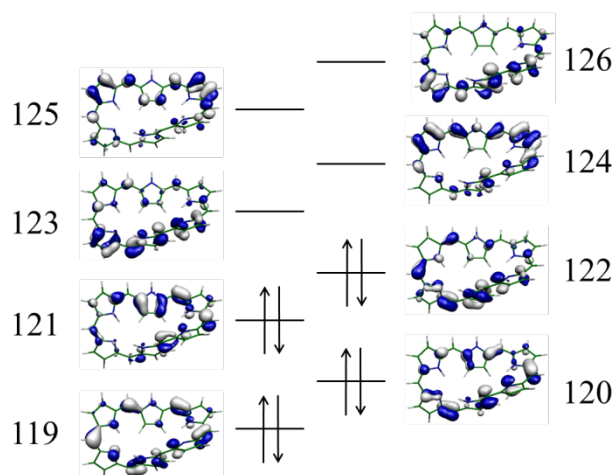


Figure S5. Molecular orbitals in the excited triplet state of the model molecule of twisted Möbius **[28]Hex** obtained by the CIS/cc-pVDZ calculation for the B3LYP/6-31G* optimized geometry. The transitions between the orbital numbers of 119 -> 125, 121 -> 123, and 122 -> 124 are regarded as the CT characters. 120 -> 126, 121 -> 124, and 122 -> 123 transitions are attributable to the LE. From the CI coefficients of 0.119, -0.212 and -0.107 for transitions 119 -> 125, 121 -> 123, and 122 -> 124, respectively, the CT character has been obtained to be 0.07 from a summation of the square values of these coefficients. Similarly, from the coefficients of 0.125, -0.337 and -0.489 for 120 -> 126, 121 -> 124, and 122 -> 123, the LE character has been obtained to be 0.369. Thus, CT:LE = 1:5 is obtained.

6. Line Shape Analyses of the TREPR Spectra

The powder pattern TREPR spectrum of the excited triplet state can be described as:

$$I(\mathbf{B}_0) = \int_0^{\pi/2} \int_0^{\pi/2} \text{Im}(\rho_{21} + \rho_{32}) D(\theta, \varphi) d\varphi d\theta \quad (\text{S1})$$

where, θ and φ are the angles between the external magnetic field (\mathbf{B}_0), ρ_{21} and ρ_{32} correspond the 1-2 and 2-3 level transitions in the density matrix of the triplet state obtained in the diagonalized sublevel system in the presence of the external magnetic field. (θ, φ) is the distribution function in the molecular orientation and is dependent on the light excitation condition.¹⁸ The distribution function (θ, φ) is described as follows:

In the case of $L // B_0$,⁸

$$\begin{aligned} D_{\parallel}(\theta, \varphi) &= \cos^2 \alpha \sin \theta \\ &= (\sin \gamma \cos \delta \sin \theta \cos \varphi + \sin \gamma \sin \delta \sin \theta \sin \varphi + \cos \gamma \cos \theta)^2 \sin \theta \quad (\text{S2}) \end{aligned}$$

In the case of $L \perp B_0$,

$$\begin{aligned} D_{\perp}(\theta, \varphi) &= \frac{1}{2} \sin^2 \alpha \sin \theta \\ &= \frac{1}{2} \{1 - (\sin \gamma \cos \delta \sin \theta \cos \varphi + \sin \gamma \sin \delta \sin \theta \sin \varphi + \cos \gamma \cos \theta)^2\} \sin \theta \quad (\text{S3}) \end{aligned}$$

where α is the angles between the \mathbf{B}_0 and \mathbf{M} as follows:

$$\mathbf{B}_0 = B_0(\sin \theta \cos \varphi, \sin \theta \sin \varphi, \cos \theta), \mathbf{M} = M(\sin \gamma \cos \delta, \sin \gamma \sin \delta, \cos \gamma)$$

The relationship between the external magnetic field (B_0) and the transition dipole moment (M) of the molecule with respect to the principal axes of the zero-field splitting tensor is illustrated in [Figure S6](#).

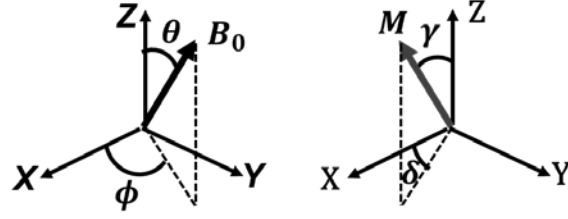


Figure S6. Relationship between the external magnetic field (B_0) and the transition dipole moment of the molecule (M) with respect to the principal axes of the zero-field splitting tensor.

To obtain the kinetic parameters of the non-radiative deactivation rate constants in the excited triplet states, we quantitatively analysed the delay time dependence of the transverse magnetizations (Figure S7) using eq.(S1) by solving the triplet sublevel populations (ρ_{11} , ρ_{22} and ρ_{33}), as follows:

$$\frac{\partial}{\partial t} \begin{pmatrix} \rho_{11} \\ \rho_{22} \\ \rho_{33} \\ \rho_{S1} \end{pmatrix} = \begin{pmatrix} -k_{12} - k_{RISC}(1) & k_{21} & 0 & k_{ISC}(1) \\ k_{12} & -k_{21} - k_{23} - k_{RISC}(2) & k_{32} & k_{ISC}(2) \\ 0 & k_{23} & -k_{32} - k_{RISC}(3) & k_{ISC}(3) \\ 0 & 0 & 0 & -k_X - k_Y - k_Z \end{pmatrix} \begin{pmatrix} \rho_{11} \\ \rho_{22} \\ \rho_{33} \\ \rho_{S1} \end{pmatrix} \quad (S4)$$

with

$$k_{ISC}(i) = |c_{iX}|^2 k_X + |c_{iY}|^2 k_Y + |c_{iZ}|^2 k_Z \quad (S5)$$

and

$$k_{RISC}(i) = |c_{iX}|^2 k_{-X} + |c_{iY}|^2 k_{-Y} + |c_{iZ}|^2 k_{-Z} \quad (S6)$$

where (c_{iX} , c_{iY} , c_{iZ}) for $i = 1, 2$ and 3 are the eigenvectors that diagonalize the spin Hamiltonian of the excited triplet state in the presence of the magnetic field. (k_X , k_Y , k_Z) and (k_{-X} , k_{-Y} , k_{-Z}) are the anisotropic S_1 - T_1 and T_1 - S_0 intersystem crossing rate constants in the spin sublevels at the zero-field. k_{ij} ($i < j$) are the spin-lattice relaxation rates between the sublevels and are treated as, $k_{ij} = k_{ji} \exp(g\beta B_0/k_B T)$ with $k_{12} = k_{23}$. The spin-lattice relaxation time is thus represented as, $T_1 = 1/(k_{ij} + k_{ji})$. The time evolution of the density matrix elements, ρ_{11} ,

ρ_{22} , ρ_{33} and ρ_{S1} can be solved by using the matrices of the eigenvectors (S) and the eigenvalues (η) of the relaxation matrix in eq.(S4) to be $\rho = S \exp(\eta t) S^{-1} \rho(t=0)$, with setting the initial population $\rho(t=0)$ dominated at the excited singlet state (ρ_{S1}). The triplet deactivation rate constant is represented as,

$$k_T = \frac{k_{-X} + k_{-Y} + k_{-Z}}{3} \quad (S7)$$

The EPR transition probabilities in T_1-T_2 and T_2-T_3 are represented as,¹⁹

$$\rho_{21} = \omega_1 \left\{ -Q_{T+} + 3C + \omega_0 - i \left(\frac{1}{T_2} \right) \right\}^{-1} (\rho_{22} - \rho_{11}) \quad (S8)$$

$$\rho_{32} = \omega_1 \left\{ -Q_{T+} - 3C + \omega_0 - i \left(\frac{1}{T_2} \right) \right\}^{-1} (\rho_{33} - \rho_{22}) \quad (S9)$$

where

$$Q_{T,+} = g_{T,eff} \beta B_0 + \frac{1}{2} \sum_i A_{T,i} M_{T,i} \quad (S10)$$

$$C = \frac{D}{6} (1 - 3 \cos^2 \theta) - \frac{E}{2} (\cos^2 \phi \sin^2 \theta - \sin^2 \phi \sin^2 \theta) \quad (S11)$$

In eq. (S10), g_T and A_T denote the effective g values and hyperfine coupling constants in the excited triplet state. In the present system, the g_T and A_T can be treated to be isotropic since the EPR spectra exhibit the symmetrical shapes. $A_T = 0$ was assumed. In eq. (S10), D and E are the ZFS constants described in the main text.

On the basis of the kinetic parameters of (k_X , k_Y , k_Z) and (k_{-X} , k_{-Y} , k_{-Z}) determined in [Figure S7](#), we also computed the delay time dependence of the sublevel populations at the zero-field, as shown in [Figure 5a](#), demonstrating that the A/A/A/E/E/E pattern is explained by the dominant T_Z depletion for the later delay times.

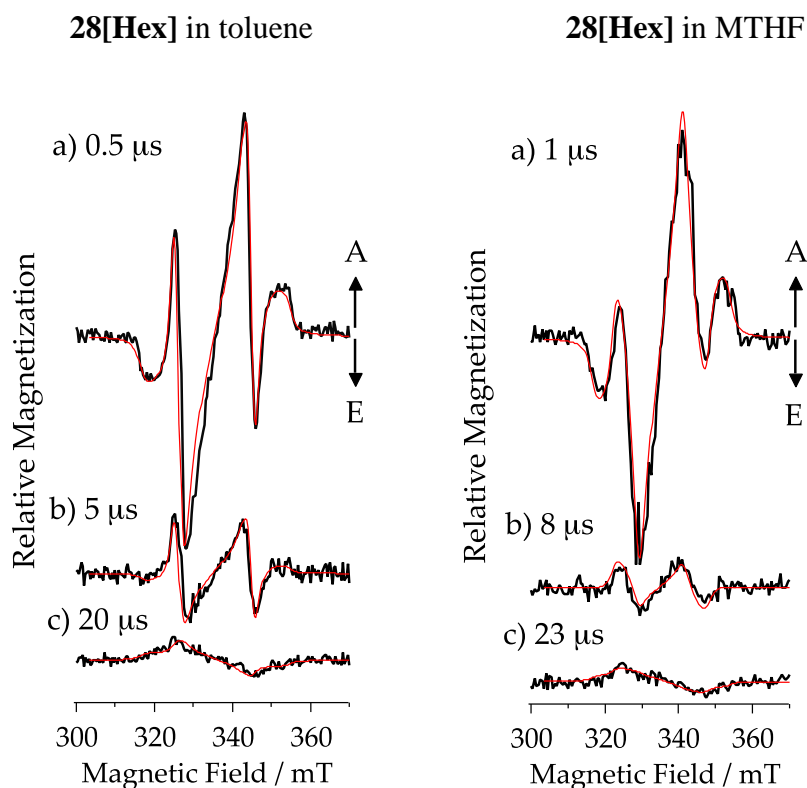


Figure S7. TREPR spectra of **28[Hex]** in toluene (left) and in MTHF (right) obtained by the depolarized laser irradiations at 77 K. The computed transverse magnetization curves are shown by the red lines to reproduce the EPR spectra together with their intensities for the given delay times. In toluene, $(k_x, k_y, k_z) = (1.0 \times 10^8, 1.2 \times 10^9, 8.0 \times 10^8) \text{ s}^{-1}$ and $(k_{-x}, k_{-y}, k_{-z}) = (1.2 \times 10^4, 1.3 \times 10^4, 2.4 \times 10^4) \text{ s}^{-1}$ were set to reproduce the data with $T_1 = 5.5 \text{ } \mu\text{s}$ as the spin-lattice relaxation time. In MTHF, $(k_x, k_y, k_z) = (1.1 \times 10^8, 3.1 \times 10^8, 3.0 \times 10^8) \text{ s}^{-1}$ and $(k_{-x}, k_{-y}, k_{-z}) = (1.3 \times 10^4, 1.1 \times 10^4, 1.9 \times 10^4) \text{ s}^{-1}$ were set with $T_1 = 7.5 \text{ } \mu\text{s}$. In MTHF, $D = -527 \text{ MHz}$ and $E = -67 \text{ MHz}$ were employed. From eq.(S7), $k_T = 1.6 \times 10^4 \text{ s}^{-1}$ and $1.4 \times 10^4 \text{ s}^{-1}$ were obtained as the triplet deactivation rate constants in toluene and MTHF, respectively.

7. ZFS parameters

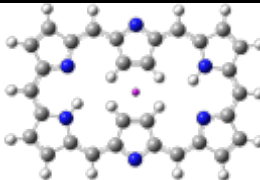
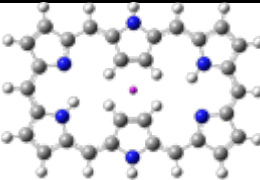
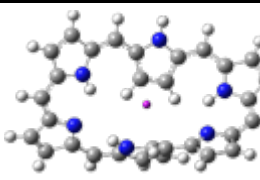
Table S1. Calculated ZFS parameters of D^{SS} and E^{SS} obtained by the CIS calculation together with the experimentally determined ZFS parameters of $D(\text{Exptl.})$ and $E(\text{Exptl.})$ obtained for the phenyl substituted porphyrins (H_2P = Tetraphenylporphyrin, ZnP = Zinc tetraphenylporphyrin, and MgP = Magnesium tetraphenylporphyrin) together with hexaphyrins (**[26]Hex** and **[28]Hex**).

	D^{SS}/MHz	E^{SS}/MHz	$ E^{SS}/D^{SS} $	$D(\text{Exptl.})/\text{MHz}$	$E(\text{Exptl.})/\text{MHz}$	$ E/D $
[26]Hex (Planar)	+971 ^a	-24 ^a	0.0258	+813 ^b	-205 ^b	0.252
[28]Hex (Möbius)	-746 ^a	-3 ^a	0.0041	-532 ^c	-18.2 ^c	0.034
H_2P	+1508 ^a	-183 ^a	0.121	1148 ^d	-239 ^d	0.209
ZnP	+1334 ^a	-54 ^a	0.040	911 ^e	-270 ^e	0.296
MgP	+1358 ^a	-78 ^a	0.057	914 ^f	-255 ^f	0.279

[a] The CIS calculations were undertaken for corresponding molecules whose phenyl groups (or pentafluorophenyl groups) are replaced with hydrogen atoms at meso positions. The CIS calculations tend to overestimate the D value for the extended π conjugated system due to the computations without the phenyl groups. However, a good correlation obeying $D^{SS} = 1.4 D(\text{Exptl.})$ is obtained between D^{SS} and $D(\text{Exptl.})$. This indicates a validity of the present computed electronic structure shown in [Figure S5](#) with CT:LE = 1:5 to explain the ZFS parameters in the twisted **[28]Hex**. It is also noted that the computed principal axes orientation (Figure 1b) of the spin-spin dipolar interaction was consistent with the experimentally determined orientation in Figure 3. [b] Obtained in 2-methyltetrahydrofuran, [c] Obtained in toluene. [d] Taken from ²⁰. Absolute sign of D was not determined experimentally. [e] Taken from ²⁰. Absolute sign of D was not determined experimentally. [f] Taken from ²⁰, absolute sign of D was not determined experimentally.

8. NICS values

Table S2. Calculated NICS values (ppm) at the ring centers in the S_0 and T_1 states of planar [26]Hex, planar [28]Hex and twisted Möbius [28]Hex.

	[26]Hex (Planar)	[28]Hex (Planar)	[28]Hex (Möbius)
NICS(0) position			
S_0	-16.75	45.88	-14.90
T_1	41.72	-17.02	59.51

9. Calculated state energies

Table S3. Calculated state energies and the energy gaps between the T_1 and S_0 states obtained by the (U)B3LYP/6-31G** methods.

	$E(S_0)$ /Hartree	$E(T_1)$ /Hartree ^a	$\Delta E(T_1-S_0)$ / eV
[26]Hex	-1483.688329	-1483.653502	0.95
[28]Hex (planar)	-1484.920999	-1484.910211	0.29
[28]Hex (twisted)	-1484.924953	-1484.884429	1.10 ^b

^a Obtained by the single point calculations for the optimized geometries in the S_0 states.

^b The vertical T_1 - S_0 energy gap has been obtained to be 1.21 eV by the (U)M05-2X/6-31G* level for the optimized geometry by M05-2X/6-31G* in the S_0 state. Since the excitation energies are not largely affected by the level of theory, T_1 - S_0 energy gap \approx 1 eV is conclusive for the twisted 28-Hex, highlighting the remarkably accelerated $T_1 \rightarrow S_0$ deactivation character by the orthogonal ${}^3\pi\pi^*$.

10. Cartesian Coordinates of Optimized Geometries

Table S4. Cartesian coordinate of B3LYP/6-31G** optimized geometry of the planar [26]Hex whose pentafluorophenyl groups are replaced with hydrogen atoms in the ground state.

Center Number	Atomic Number	Atomic Type	Coordinates (Angstroms)		
			X	Y	Z
1	6	0	1.106678	2.917939	0.184994
2	6	0	0.691849	1.589754	0.656693
3	6	0	-0.662921	1.597131	0.645802
4	7	0	-3.808521	1.434611	0.041082
5	6	0	-1.058534	2.924584	0.166768
6	6	0	-2.343431	3.434130	-0.050762
7	7	0	3.808521	-1.434611	-0.041082
8	6	0	-3.581766	2.777149	-0.046001
9	6	0	-5.162999	1.293088	0.001993
10	6	0	-5.837448	0.064878	0.025410
11	6	0	-5.247956	-1.198535	0.028807
12	6	0	-5.886061	-2.478159	0.105943
13	7	0	0.028637	3.706267	-0.061289
14	6	0	-4.904077	-3.434708	0.122428
15	6	0	-3.629070	-2.780904	0.028632
16	6	0	-2.393655	-3.430325	0.017176
17	6	0	-1.106678	-2.917939	-0.184994
18	6	0	-0.691849	-1.589754	-0.656693
19	6	0	0.662921	-1.597131	-0.645802
20	6	0	1.058534	-2.924584	-0.166768
21	7	0	-3.893129	-1.428599	-0.029099
22	6	0	2.343431	-3.434130	0.050762
23	6	0	3.581766	-2.777149	0.046001
24	6	0	5.162999	-1.293088	-0.001993
25	6	0	5.837448	-0.064878	-0.025410
26	6	0	5.247956	1.198535	-0.028807
27	6	0	5.886061	2.478159	-0.105943
28	6	0	4.904077	3.434708	-0.122428
29	6	0	3.629070	2.780904	-0.028632
30	6	0	2.393655	3.430325	-0.017176

31	7	0	-0.028637	-3.706267	0.061289
32	6	0	-4.842947	3.512010	-0.154811
33	6	0	-5.831770	2.587099	-0.102431
34	7	0	3.893129	1.428599	0.029099
35	6	0	4.842947	-3.512010	0.154811
36	6	0	5.831770	-2.587099	0.102431
37	1	0	1.332078	0.790960	1.004451
38	1	0	-1.341892	0.820800	0.961502
39	1	0	-2.370321	4.498061	-0.272274
40	1	0	-4.930332	4.587470	-0.239542
41	1	0	-6.902400	2.740262	-0.144818
42	1	0	-6.922456	0.089267	0.035176
43	1	0	-3.248584	-0.641487	-0.018479
44	1	0	-6.955948	-2.626821	0.150936
45	1	0	-5.026823	-4.507611	0.174998
46	1	0	-2.429951	-4.495924	0.223963
47	1	0	-1.332078	-0.790960	-1.004451
48	1	0	1.341892	-0.820800	-0.961502
49	1	0	2.370321	-4.498061	0.272274
50	1	0	4.930332	-4.587470	0.239542
51	1	0	6.902400	-2.740262	0.144818
52	1	0	6.922456	-0.089267	-0.035176
53	1	0	3.248584	0.641487	0.018479
54	1	0	6.955948	2.626821	-0.150936
55	1	0	5.026823	4.507611	-0.174998
56	1	0	2.429951	4.495924	-0.223963

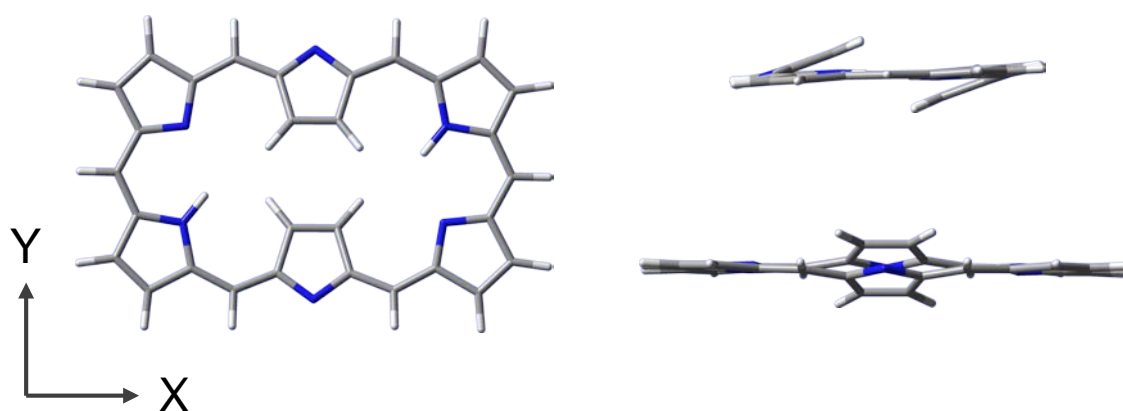


Table S5. Cartesian coordinate of B3LYP/6-31G** optimized geometry of the twisted Möbius [28]Hex whose pentafluorophenyl groups are replaced with hydrogen atoms in the ground state.

Center Number	Atomic Number	Atomic Type	Coordinates (Angstroms)		
			X	Y	Z
1	6	0	5.294390	0.264498	-0.257046
2	6	0	6.207243	1.273641	-0.716129
3	1	0	7.284221	1.212805	-0.638420
4	6	0	5.466157	2.323380	-1.205216
5	1	0	5.837423	3.260244	-1.598314
6	6	0	4.071362	1.995196	-1.070278
7	6	0	2.962736	2.829103	-1.220946
8	6	0	1.631513	2.451404	-0.964787
9	6	0	1.006298	1.173655	-0.978276
10	1	0	1.464406	0.255566	-1.313167
11	6	0	-0.301729	1.316025	-0.558084
12	1	0	-1.020835	0.515311	-0.486417
13	6	0	-0.534414	2.687582	-0.253937
14	6	0	-1.617620	3.355995	0.332713
15	6	0	-2.840030	2.841137	0.765789
16	6	0	-3.875149	3.577974	1.435350
17	1	0	-3.797210	4.623389	1.701920
18	6	0	-4.938698	2.737772	1.656944
19	1	0	-5.880860	2.979391	2.129301
20	6	0	-4.606142	1.454057	1.116208
21	6	0	-5.413337	0.333763	0.924898
22	6	0	-5.030655	-0.803644	0.188585
23	6	0	-5.960187	-1.696964	-0.485859
24	1	0	-7.036131	-1.694197	-0.364703
25	6	0	-5.213603	-2.448264	-1.343720
26	1	0	-5.554554	-3.206981	-2.036750
27	6	0	-3.828393	-2.076315	-1.114384
28	6	0	-2.714373	-2.629715	-1.755716
29	6	0	-1.393403	-2.549402	-1.299635
30	6	0	-0.176348	-2.836832	-1.986904
31	1	0	-0.119052	-3.152205	-3.019818
32	6	0	0.871550	-2.639374	-1.115299
33	1	0	1.926087	-2.781660	-1.294394

34	6	0	0.331238	-2.294074	0.166194
35	6	0	0.982292	-2.289654	1.411010
36	6	0	2.365009	-2.127568	1.573918
37	6	0	3.174829	-2.636531	2.672045
38	1	0	2.803619	-3.180228	3.531735
39	6	0	4.472285	-2.361256	2.351571
40	1	0	5.362322	-2.603333	2.918930
41	6	0	4.432164	-1.590355	1.115664
42	6	0	5.497744	-0.850916	0.558208
43	7	0	4.031818	0.716856	-0.569477
44	1	0	3.233454	0.176592	-0.221274
45	7	0	0.646128	3.345838	-0.579174
46	1	0	0.836267	4.301964	-0.321890
47	7	0	-3.317255	1.555562	0.631148
48	1	0	-2.927718	0.762281	0.125864
49	7	0	-3.745309	-1.083922	-0.171396
50	7	0	-1.036485	-2.218249	-0.007309
51	1	0	-1.724260	-1.904581	0.666324
52	7	0	3.154274	-1.495300	0.657666
53	1	0	-6.449078	0.415255	1.238612
54	1	0	-2.877047	-3.180136	-2.677609
55	1	0	-1.494073	4.422286	0.505656
56	1	0	3.170716	3.876577	-1.421768
57	1	0	6.509682	-1.054371	0.892727
58	1	0	0.384034	-2.495360	2.295971

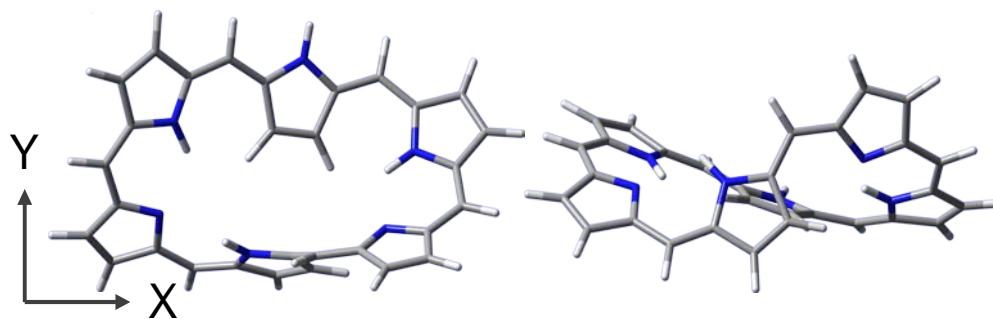
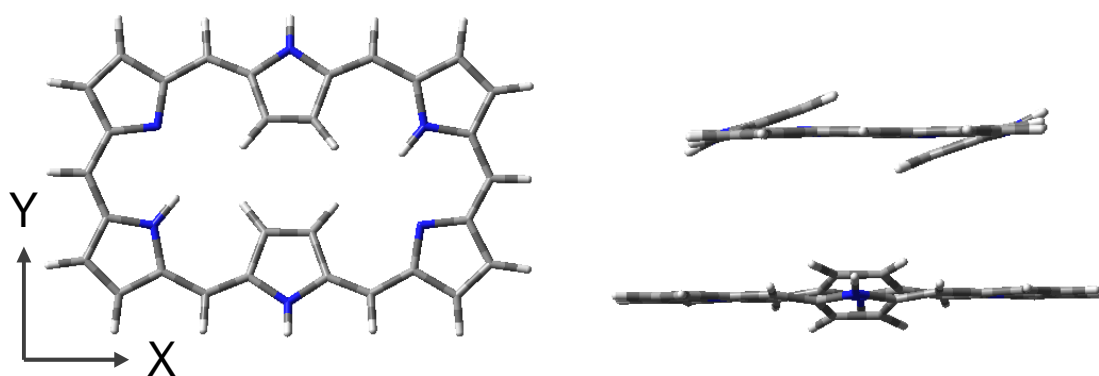


Table S6. Cartesian coordinate of B3LYP/6-31G** optimized geometry of the planer [28]Hex whose pentafluorophenyl groups are replaced with hydrogen atoms in the ground state.

Center Number	Atomic Number	Atomic Type	Coordinates (Angstroms)		
			X	Y	Z
1	6	0	1.181631	2.948964	0.141404
2	6	0	0.700926	1.656678	0.595236
3	6	0	-0.660903	1.663075	0.585129
4	7	0	-3.848801	1.446056	0.023578
5	6	0	-1.122704	2.956901	0.123279
6	6	0	-2.383519	3.452730	-0.084531
7	7	0	3.848800	-1.446056	-0.023585
8	6	0	-3.643432	2.768191	-0.043826
9	6	0	-5.234174	1.288709	0.012575
10	6	0	-5.893684	0.077307	0.017227
11	6	0	-5.321886	-1.214618	0.017259
12	6	0	-5.958981	-2.469135	0.058062
13	7	0	0.031768	3.707277	-0.068845
14	6	0	-4.966267	-3.446270	0.073493
15	6	0	-3.710498	-2.799102	0.030490
16	6	0	-2.440635	-3.453062	0.057581
17	6	0	-1.181632	-2.948964	-0.141399
18	6	0	-0.700927	-1.656678	-0.595231
19	6	0	0.660901	-1.663076	-0.585128
20	6	0	1.122704	-2.956902	-0.123270
21	7	0	-3.959754	-1.450878	-0.007341
22	6	0	2.383518	-3.452730	0.084531
23	6	0	3.643432	-2.768191	0.043822
24	6	0	5.234173	-1.288710	-0.012579
25	6	0	5.893683	-0.077307	-0.017230
26	6	0	5.321885	1.214618	-0.017259
27	6	0	5.958997	2.469135	-0.058063
28	6	0	4.966267	3.446271	-0.073489
29	6	0	3.710498	2.799103	-0.030486
30	6	0	2.440634	3.453061	-0.057575
31	7	0	-0.031769	-3.707275	0.068853
32	6	0	-4.902417	3.506537	-0.104270
33	6	0	-5.894011	2.579051	-0.055486

34	7	0	3.959753	1.450878	0.007346
35	6	0	4.902416	-3.506536	0.104265
36	6	0	5.894011	-2.579052	0.055475
37	1	0	0.038305	4.592361	-0.550166
38	1	0	1.332287	0.852828	0.945754
39	1	0	-1.329697	0.880046	0.905434
40	1	0	-2.452024	4.511420	-0.326752
41	1	0	-4.993401	4.583796	-0.163705
42	1	0	-6.964829	2.736777	-0.076066
43	1	0	-6.979778	0.106386	0.013588
44	1	0	-3.313981	-0.666575	0.019509
45	1	0	-7.029498	-2.619490	0.077861
46	1	0	-5.100172	-4.518682	0.099760
47	1	0	-2.505770	-4.513231	0.290769
48	1	0	-0.038305	-4.592366	0.550162
49	1	0	-1.332287	-0.852828	-0.945749
50	1	0	1.329695	-0.880048	-0.905436
51	1	0	2.452024	-4.511419	0.326755
52	1	0	4.993401	-4.583795	0.163701
53	1	0	6.964828	-2.736778	0.076051
54	1	0	6.979777	-0.106386	-0.013593
55	1	0	3.313980	0.666574	-0.019503
56	1	0	7.029496	2.619490	-0.077865
57	1	0	5.100171	4.518683	-0.099756
58	1	0	2.505768	4.513231	-0.290761



References

1. (a) Shin, J.-Y.; Furuta, H.; Yoza, K.; Igarashi, S.; Osuka, A., m eso-Aryl-Substituted Expanded Porphyrins. *J. Am.Chem.Soc.* **2001**, *123* (29), 7190-7191; (b) Neves, M. G.; Martins, R. M.; Tomé, A. C.; Silvestre, A. J.; Silva, A. M.; Félix, V.; Cavaleiro, J. A.; Drew, M. G., meso-Substituted expanded porphyrins: new and stable hexaphyrins. *Chem. Commun.* **1999**, (4), 385-386.
2. Fuki, M.; Murai, H.; Tachikawa, T.; Kobori, Y., Time Resolved EPR Study on the Photoinduced Long-Range Charge-Separated State in Protein: Electron Tunneling Mediated by Arginine Residue in Human Serum Albumin. *J. Phys.Chem. B* **2016**, *120* (19), 4365-4372.
3. (a) Becke, A. D., Density-functional thermochemistry. III. The role of exact exchange. *J. Chem. Phys.* **1993**, *98* (7), 5648-5652; (b) Lee, C.; Yang, W.; Parr, R., Density-functional exchange-energy approximation with correct asymptotic behaviour. *Phys. Rev. B* **1988**, *37*, 785-789; (c) Miehlich, B.; Savin, A.; Stoll, H.; Preuss, H., Results obtained with the correlation energy density functionals of Becke and Lee, Yang and Parr. *Chem. Phys. Lett.* **1989**, *157* (3), 200-206.
4. (a) Petersson, G.; Al-Laham, M. A., A complete basis set model chemistry. II. Open-shell systems and the total energies of the first-row atoms. *J. Chem. Phys.* **1991**, *94* (9), 6081-6090; (b) Petersson, a.; Bennett, A.; Tensfeldt, T. G.; Al-Laham, M. A.; Shirley, W. A.; Mantzaris, J., A complete basis set model chemistry. I. The total energies of closed-shell atoms and hydrides of the first-row elements. *J. Chem. Phys.* **1988**, *89* (4), 2193-2218.
5. Frisch, M., Gaussian 03, Revision D. 01; Gaussian, Inc: Wallingford, CT, **2004**.
6. Ortiz, J.; Cioslowski, J.; Fox, D., Gaussian 09, Revision B. 01; Gaussian, Inc.: Wallingford, CT, **2009**.
7. Ridley, J.; Zerner, M., An intermediate neglect of differential overlap technique for spectroscopy: pyrrole and the azines. *Theoret. Chim. Acta* **1973**, *32* (2), 111-134.
8. Bacon, A. D.; Zerner, M. C., An intermediate neglect of differential overlap theory for transition metal complexes: Fe, Co and Cu chlorides. *Theoret. Chim.Acta* **1979**, *53* (1), 21-54.
9. Neese, F., The ORCA program system. *Wiley Interdisciplinary Reviews: Computational Molecular Science* **2012**, *2* (1), 73-78; Neese, F.; Becker, U.; Ganyushin, G.; Hansen, A.; Izsak, R.; Liakos, D.; Kollmar, C.; Kossmann, S.; Pantazis, D.; Petrenko, T., ORCA: An ab Initio, DFT, and Semiempirical SCF-MO Package, version 3.0. *University of Bonn* **2012**.
10. Foresman, J. B.; Head-Gordon, M.; Pople, J. A.; Frisch, M. J., Toward a systematic molecular orbital theory for excited states. *J. Phys. Chem.* **1992**, *96* (1), 135-149.
11. Woon, D. E.; Dunning Jr, T. H., Gaussian basis sets for use in correlated molecular calculations. III. The atoms aluminum through argon. *J. Chem. Phys.* **1993**, *98* (2), 1358-1371.
12. (a) Sinnecker, S.; Neese, F., Spin– Spin Contributions to the Zero-Field Splitting Tensor in Organic Triplets, Carbenes and Biradicals A Density Functional and Ab Initio Study. *J. Phys. Chem. A* **2006**, *110* (44), 12267-12275; (b) McWeeny, R.; Mizuno, Y. In *The density matrix in many-electron quantum mechanics II. Separation of space and spin variables; spin coupling problems*, Proc. R. Soc. Lond. A, **1961**, 554-577; (c) Shoji, M.; Koizumi, K.; Hamamoto, T.; Taniguchi, T.; Takeda, R.; Kitagawa, Y.; Kawakami, T.; Okumura, M.; Yamanaka, S.; Yamaguchi, K., A theoretical study of zero-field splitting of organic biradicals. *Polyhedron* **2005**, *24* (16-17), 2708-2715.
13. Sugisaki, K.; Toyota, K.; Sato, K.; Shiomi, D.; Kitagawa, M.; Takui, T., Ab initio calculations of spin–orbit contribution to the zero-field splitting tensors of $n\pi^*$ excited states

by the CASSCF method with MRMP2 energy correction. *Chem. Phys. Lett.* **2009**, *477* (4-6), 369-373.

14. (a) Tanabe, M.; Matsuoka, H.; Ohba, Y.; Yamauchi, S.; Sugisaki, K.; Toyota, K.; Sato, K.; Takui, T.; Goldberg, I.; Saltsman, I., Time-resolved electron paramagnetic resonance and phosphorescence studies of the lowest excited triplet states of Rh (III) corrole complexes. *J. Phys.Chem. A* **2012**, *116* (39), 9662-9673; (b) Yamauchi, S.; Tanabe, M.; Ohba, Y.; Sugisaki, K.; Toyota, K.; Sato, K.; Takui, T.; Saltsman, I., Complete assignment of spin sublevels in the lowest excited triplet state of corrole compounds by time-resolved EPR spectroscopy. *Chem. Phys. Lett.* **2012**, *521*, 64-68.

15. (a) Wolinski, K.; Hinton, J. F.; Pulay, P., Efficient implementation of the gauge-independent atomic orbital method for NMR chemical shift calculations. *J. Am. Chem.Soc.* **1990**, *112* (23), 8251-8260; (b) Gauss, J., Effects of electron correlation in the calculation of nuclear magnetic resonance chemical shifts. *J. Chem. Phys.* **1993**, *99* (5), 3629-3643.

16. Sankar, J.; Mori, S.; Saito, S.; Rath, H.; Suzuki, M.; Inokuma, Y.; Shinokubo, H.; Suk Kim, K.; Yoon, Z. S.; Shin, J.-Y., Unambiguous Identification of Möbius Aromaticity for meso-Aryl-substituted [28] hexaphyrins (1.1. 1.1. 1.1). *J. Am.Chem.Soc.* **2008**, *130* (41), 13568-13579.

17. Oh, J.; Sung, Y. M.; Kim, W.; Mori, S.; Osuka, A.; Kim, D., Aromaticity Reversal in the Lowest Excited Triplet State of Archetypical Möbius Heteroannulenic Systems. *Angew. Chem.Int. Ed.* **2016**, *55* (22), 6487-6491.

18. (a) Frank, H. A.; Bolt, J.; Friesner, R.; Sauer, K., Magnetophotoselection of the triplet state of reaction centers from Rhodospseudomonas sphaeroides R-26. *Biochim. Biophys. Acta-Bioenergetics* **1979**, *547* (3), 502-511; (b) Thurnauer, M. C.; Norris, J. R., The ordering of the zero field triplet spin sublevels in the chlorophylls. A magnetophotoselection study. *Chem. Phys. Lett.* **1977**, *47* (1), 100-105; (c) Borovykh, I. V.; Proskuryakov, I. I.; Klenina, I. B.; Gast, P.; Hoff, A. J., Magnetophotoselection study of the lowest excited triplet state of the primary donor in photosynthetic bacteria. *J. Phys. Chem. B* **2000**, *104* (17), 4222-4228.

19. Wasserman, E.; Snyder, L.; Yager, W., ESR of the triplet states of randomly oriented molecules. *J. Chem. Phys.* **1964**, *41* (6), 1763-1772.

20. Kamata, Y.; Akiyama, K.; Tero-Kubota, S.; Tabata, M., Two-laser two-color time-resolved EPR study on higher-excited-state triplet-singlet intersystem crossing of porphyrins and phthalocyanines. *Appl. Mag. Reson.* **2003**, *23* (3-4), 409.